Closed-loop magnetic separation of nanoparticles on a packed bed of spheres

Cécilia Magnet, Mesferdon Akouala, Pavel Kuzhir, Georges Bossis, A Zubarev, Norman Wereley

Closed-loop magnetic separation of nanoparticles on a packed bed of spheres

Cécilia Magnet[1], Mesferdon Akouala[1], Pavel Kuzhir[1], Georges Bossis[1], A. Zubarev[2], and Norman M. Wereley[3]

[1]*University of Nice-Sophia Antipolis, UMR 7336, Laboratory of Condensed Matter Physics, 28, avenue Joseph Vallot, Nice,06100, France.*

[2]*Urals Federal University, Lenina Ave 51, 620083, Ekaterinburg, Russia*

[3]*3179F Glenn L Martin Hall, Department of Aerospace Engineering, University of Maryland, College Park, MD 20742, USA*

Abstract

In this work, we consider magnetic separation of iron oxide nanoparticles when a nanoparticle suspension (diluted ferrofluid) passes through a closed-loop filter composed of a packed bed of micro-beads magnetized by an externally applied magnetic field. We show that the capture of nanoparticles of a size as small as 60 nm is easily achieved at low-to-moderate magnetic fields (15 kA/m) thanks to relatively strong magnetic interactions between them. The key parameter governing the capture process is the Mason number - the ratio of hydrodynamic-to-magnetic forces exerted to nanoparticles. The filter efficiency, Λ, defined through the ratio of the inlet-to-outlet concentration shows a power-law dependency on Mason number, $\Lambda \propto Ma^{-0.83}$, in the range $10^2 < Ma < 10^4$. The proposed theoretical model allows a correct prediction of the Mason number dependency of the filter efficiency. The obtained results could be of potential interest for water purification systems based on chemical adsorption of micro-pollutants on magnetic nanoparticles, followed by magnetic separation of the nanoparticles.

I. Introduction

Separation of magnetic particles from a suspending liquid and/or other substances has found numerous applications in different technologies related to the ore beneficiation[1], separation biological cells or molecules[2], and water or soil purification from micro-pollutants[3]. Sub-micron particles posses a high specific surface, and allow a more efficient adsorption of micro-pollutant or biological molecules, as compared to conventionally used micron-sized magnetic beads. However, the magnetic separation of nanoparticles as small as 20-50 nm in size has been for a long time considered to be inefficient because of a strong Brownian motion[4]. We have recently shown that the nanoparticles can still be efficiently

separated if magnetic interactions between them are strong enough to induce a phase separation. Upon an application of an external magnetic field, the nanoparticles reversibly gather into drop-like aggregates, which are extracted from the suspending liquid much easily than individual nanoparticles[5]. In or previous works[5,6], we have studied in details the capture of iron oxide nanoclusters by a single collector – an iron or nickel micro-bead magnetized by an external applied magnetic field. The nanoclusters were permanent quasi-spherical agglomerates of individual nanoparticles stabilized in water by an oleic acid double layer. We have shown that, at strong magnetic interactions (described by the dipolar coupling parameter - the ratio of magnetic-to-thermal energy, α>3) the capture process of relatively small (about 60 nm) nanoclusters is in principally governed by hydrodynamic and magnetic forces acting on them, or by their ratio called Mason number.

In the present paper, we study nanocluster accumulation around multiple magnetized collectors – a packed bed of microbeds. We seek to realize an effective nanoparticle filtration at magnetic fields as low as 30 kA/m as opposed to standard high gradient magnetic separators (HGMS) conventionally used in this domain[7]. Our goal is to establish the effect of the neighbouring collectors on the accumulation process occurred on a considered collector and to provide the Mason number effect on the filtration efficiency as a macroscopic feature of the filtration on porous medium. We start with description of the experimental setup in Section II. Then, in Section III, we develop a theoretical model allowing predictions of the capture efficiency both in microscopic (pore size) and macroscopic (whole filter) scales. Finally, in Section IV, we compare experimental results with our model and establish relationships between the filter efficiency and the Mason number.

II. Experimental setup

In the experiment, the nanocluster suspension is subjected to a recirculation flow in a closed loop circuit containing a magnetic filter whose ends are connected with each other by flexible tubes, as depicted in Fig. 1. A peristaltic pump Masterflex 7520-47 (COLE PARMER Instrument Company) is included into the circuit and ensures the flow with a constant flow rate Q corresponding to the suspension speeds, $u = 4Q/(\pi D_{filter}^2)$, inside the filter, ranging from 0.03 to 0.12m/s, with D_{filter} being the filter diameter.

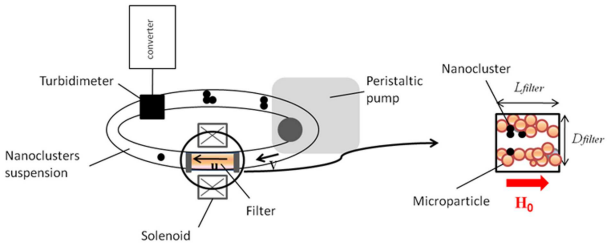

Fig. 1 (Color online). Sketch of the experimental setup

The filter presents a cylindrical column, of a length L_{filter}=19.2 mm and a diameter D_{filter}=6.91 mm, and filled with nickel microbeads of a mean diameter d_m=45±5 µm at a volume fraction of about 30%, which corresponds to the filter porosity $\varepsilon\approx0.7$. The size of the flexible tubes connecting both filter ends is D_{tube}=6.35 mm and $L_{tube}\approx$0.6m. A solenoid is placed around the filter and generates a magnetic field parallel to the flow direction and having an intensity up to H_0=32 kA/m. The nanocluster suspension is prepared by dilution of the steric ferrofluid (whose synthesis is described in Magnet *et al.*[5]) by a distilled water at a solid phase concentration ϕ_0=0.0016%.

Once the field is applied and the flow is started, the filter becomes to capture the nanoclusters such that their concentration ϕ outside the filter (in the tubes) starts to decrease with the time. The temporal evolution of the concentration is measured by a turbidimeter introduced in the circuit and transmitting the data to a personal computer. The turbidimeter Mettler Toledo DP Phototrode measures the transmittance of a light beam, which is then converted to the particle concentration ϕ using an appropriate calibration curve. In experiments, we analyse the effect of the filtration speed u and of the applied field H_0 on the concentration evolution $\phi(t)$. A deeper understanding of the field and velocity effects on the filtration process may be achieved through theoretical considerations developed in the next section.

III. Theory

The common method to describe the physics of filtration consists of considering two different scales. In the macroscopic scale, the filter is considered as a continuum medium characterised by two phenomenological parameters: the filter efficiency, Λ, and the maximal retention capacity, σ_m. The concentration evolution inside the filter, $\phi(t,z)$, is described by the mass conservation. In the microscopic scale, the particle motion is considered in a pore size scale and the parameters Λ and σ_m are calculated as function of the Mason number. Following

this scheme, we establish the relationship between the filter efficiency Λ and the Mason number *Ma*.

Let us first consider the filtration of a magnetic particle suspension through a cylindrical filter (macroscopic scale) of a constant cross-section and having a length L_{filter}, as depicted in Fig. 2. A Cartesian coordinate system is introduced with the origin O situated at the filter inlet and the axis O*z* being the axis of symmetry oriented along the flow direction. The superficial velocity *u* (called also the filtration velocity) is constant during time *t* and does not vary along the O*z* axis. At this macroscopic scale, we seek for the temporal evolution $\phi(t)$ of the nanoclusters concentration.

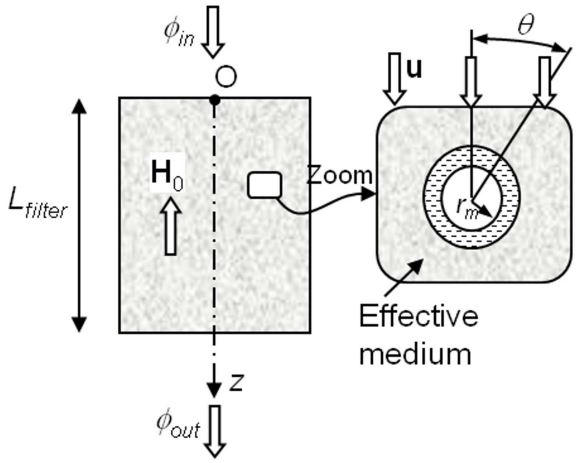

Fig. 2. Schematic geometry for the filtration of the magnetic particle suspension at the macroscopic (left) and the microscopic (right) scales

The starting point of the model is the particle mass conservation in the filter. The averaging of the mass balance over a representative volume at a microscopic scale gives the so-called filtration equations, describing the concentration distribution inside the filter at a macroscopic scale[8,9]:

$$\frac{\partial \sigma}{\partial z} = -\lambda F(\sigma)\sigma \tag{1}$$

$$\frac{d\sigma_{in}}{d\tau} = u\lambda F(\sigma_{in})\phi_{in}(\tau) \tag{2}$$

$$\frac{\phi(\tau,z)}{\phi_{in}(\tau)} = \frac{\sigma(\tau,z)}{\sigma_{in}(\tau)} \tag{3}$$

where σ is the concentration of deposited particles (ratio of the total volume of captured particles to the filter volume); ϕ_{in} and σ_{in} are concentrations of non-captured and deposited

particle at the filter inlet; $\tau(t,z) = t - \int_0^z (\varepsilon / u) dz$ is the corrected time; ε is the filter porosity; λ is the phenomenological filter coefficient corresponding to the capture efficiency of a clear filter; $F(\sigma) = 1 - \sigma / \sigma_m$ is the correction factor taking into account a decrease of the capture efficiency with a progressive particle deposition on the filter elements; σ_m is the maximum concentration of deposited particles when the filter is saturated; this quantity is called hereinafter the retention capacity.

In the present case of the closed loop filter [Fig. 1], the particle flux balance along the connecting tube implies that the particle concentration at the filter outlet at the moment *t* is the same as the particle concentration at the filter inlet at the time $t + \delta$, with $\delta = L_{tube} / u_{tube}$ being the transit time along the connecting tube of a length L_{tube}, in other words, $\phi_{out}(t) = \phi_{in}(t + \delta)$. Thus, the following initial conditions should be associated to the filtration equations (1)-(3): $\sigma(\tau, z = 0) = \sigma_{in}(\tau)$; $\sigma_{in}(\tau = 0) = 0$; $\phi_{out}(\tau) = \phi_{in}(\tau + \Delta)$; and $\phi_{in}(\tau = 0) = \phi_0$, where ϕ_0 is the initial particle concentration in the circuit, $\Delta = V_{tot} / Q$ is the walk time that the particle put to run the full cycle, and $V_{tot} = V_{tube} + \varepsilon V_{filter}$ is the circuit volume. The filter porosity ε and the filtration velocity *u* are considered to be constant.

An analytical solution of the system (1)-(3) can be obtained in the limiting case of high velocities resulting in relatively low filter efficiency, $\Lambda = \lambda L_{filter} \ll 1$, and in a large number of circulation cycles, or equivalently, $\Delta / \tau \ll 1$. This situation is practically relevant and the formulated restrictions are satisfied in most of our experiments. The second restriction allows us to develop the inlet particle concentration $\phi_{in}(\tau + \Delta)$ in a power series on Δ keeping only the first two terms:

$$\phi_{in}(\tau + \Delta) = \phi_{in}(\tau) + \frac{d\phi_{in}}{d\tau}\Delta + o(\Delta^2) \qquad (4)$$

Substituting the last equation into the system of equations (1)-(3), we obtain, after some mathematics, the following solution for the temporal evolution of the inlet particle concentration for the closed loop filter:

$$\frac{\phi_{in}}{\phi_0} = \frac{\gamma_2 \exp(-\kappa\gamma_2\Lambda T)}{1 - (1 - \gamma_2)\exp(-\kappa\gamma_2\Lambda T)} \qquad (5)$$

Here $T = u\tau / L_{filter} \approx ut / L_{filter} - \varepsilon$ is the dimensionless time scaled by the time of the particle walk along the filter, $\kappa = V_{filter} / V_{tot} = V_{filter} / (V_{tube} + \varepsilon V_{filter})$ is the geometrical parameter of the

circuit and γ_2 is the dimensionless retention capacity of the filter related to the dimensional retention capacity σ_m by the expression: $\gamma_2 = 1 - \phi_0/(\kappa\sigma_m)$. Since the concentration varies slowly with time (at the considered time scale, $\tau \gg \Delta$), Eq. (5) gives a correct estimation of the particle concentration at any point of the circuit and not only at the filter inlet.

The next step is to model the filtration process on a microscopic scale. We develop the simplest approach allowing taking into account the influence of the neighbouring collectors on the capture process on a given collector. Namely, we adopt the Happel's model[10], in which an elementary cell of the porous filter is represented by two concentric spheres, as depicted schematically in Fig. 2. The inner sphere (of a radius r_m) stands for an individual collector, and the nanocluster suspension flows in the envelope between the spheres. The rest of the filter is represented by an effective medium situated outside the outer sphere (of a radius $b = r_m(1-\varepsilon)^{-1/3}$). We consider a Stokes flow of the suspension of magnetic particles (nanoclusters) through the cell. The velocity at the cell entrance is imposed by the Happel's boundary conditions (radial component at the outer sphere is $v_c = -u\cos\theta$ and the shear rate is zero, $(1/r)\partial v_r/\partial\theta + r\partial(v_\theta/r)/\partial\theta = 0$, with θ – the polar angle, cf. Fig. 2). The external uniform magnetic field is oriented along the main flow (direction of the superficial velocity **u**). For this geometry, the filter efficiency Λ is related to the capture efficiency, e_{coll}, of the individual collector by the following expression[8]:

$$\Lambda = \frac{3}{4}(1-\varepsilon)^{1/3}\frac{L_{filter}}{r_m}e_{coll} \qquad (6)$$

The capture efficiency e_{coll} of a single collector can be found by an analysis of trajectories of magnetic particles passing through the concentric sphere cell. Due to demagnetizing effects, the collector (inner sphere) perturbs the magnetic field lines around it and creates the field gradients in the vicinity of its surface. These field gradients exert a force on the magnetic nanoclusters arriving with the suspension flow. Some of them will be entrapped by the collector. Mathematical details of this analysis are described in the work of Moyer et al.[11] for the considered geometry. Briefly, the particle trajectory follows from the equilibrium of magnetic and hydrodynamic forces, and Brownian motion of particles is neglected because of sufficiently high values of the dipolar coupling parameter, $\alpha > 5$, encountered in experiments. Therefore, in the absence of colloidal interactions, the unique dimensionless parameter governing the capture process is the Mason number defined by the following formula:

$$Ma \equiv \frac{3\eta_0 u r_m}{\beta_n \mu_0 H_0^{\,2} r_n^{\,2}} \qquad (7)$$

where η_0 is the solvent (water) viscosity; r_n is the nanocluster radius; $\beta_n = \chi_n/(\chi_n + 3) \approx 0.75$ is the magnetic contrast factor, $\chi_n \approx 9$ is the nanocluster magnetic susceptibility; H_0 is the intensity of the external uniform magnetic field.

The nanocluster trajectories calculated numerically for Mason number Ma=100 are plotted in Fig.3. The black trajectory with the starting point θ_0<0.407 arrives on the collector indicating that the nanocluster has been captured. The trajectories at θ_0>0.407 do not intercept the microsphere surface and leave the flow cell; the nanoclusters describing these trajectories are not captured. The red trajectory for $\theta_0=\theta_c$=0.407 is the so-called critical trajectory separating the fluxes of captured and non-captured particles. The collector efficiency e_{coll} is defined as a ratio of the flux of captured particles to the total particle flux entering the cell; it is related to the starting angle of the limiting trajectory by the following expression: $e_{coll} = \sin^2 \theta_c$. Finally, analysis of the critical trajectories at different Mason numbers allows us to find the Mason number dependency of the collector efficiency as well as of the filter efficiency through Eq. (6).

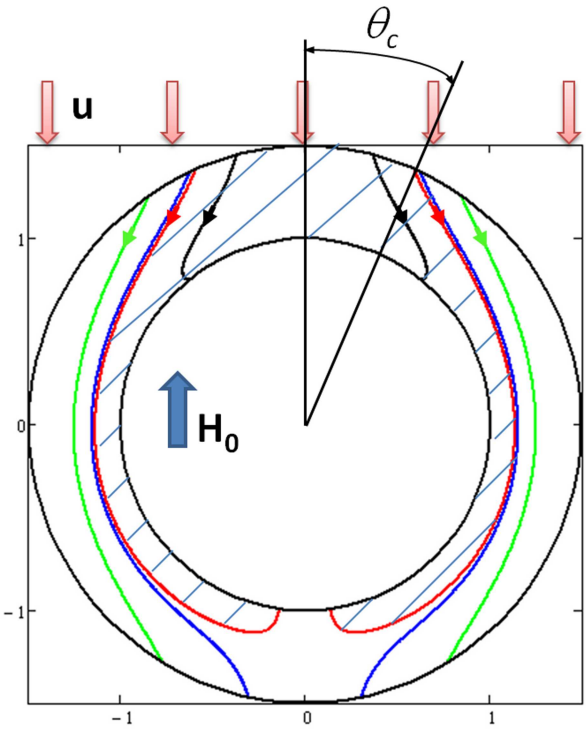

Fig. 3. (Color online). Nanocluster trajectories around a spherical collector in frames of the Happel's concentric sphere model[10]. The filtration flow is oriented downwards and the external magnetic field is longitudinal. The critical trajectory (red line) delimits the hatched zone of captured nanoclusters.

In the wide range of Mason numbers used in our experiments, the filter efficiency, Λ, is successfully fitted by a power law, as follows:

$$\Lambda = \begin{cases} \dfrac{3}{4}\dfrac{(1-\varepsilon)^{1/3}}{\varepsilon^2}\dfrac{L_{filter}}{r_m} 3.65 Ma^{-0.83} & \text{at} \quad 10^2 < Ma < 10^4 \\ \dfrac{3}{4}\dfrac{(1-\varepsilon)^{1/3}}{\varepsilon^2}\dfrac{L_{filter}}{2r_m} 48 Ma^{-1} & \text{at} \quad Ma > 10^4 \end{cases} \tag{8}$$

The Ma^{-1} behaviour is confirmed by analytical calculations in the range of very high Mason numbers. For weak Mason numbers, Ma <1 and high filter porosities, $\varepsilon \approx 1$, we recover the behaviour $\Lambda \propto Ma^{-0.5}$ predicted by Friedlander and al.[12] for an isolated collector placed in an unbounded volume of a magnetic suspension.

The microscopic model described in this Section relates the capture efficiency of the whole filter Λ to the Mason number. The full description of the filtration process requires a relationship between the retention capacity of the filter σ_m or γ_2 and the Mason number. However, we do not pursue this goal because this quantity cannot be precisely determined by fitting the experimental curves and we were unable to measure it independently. We suppose that the retention capacity decreases with Mason number because the nanoclusters are more easily washed away from the filter.

IV. Experimental results and comparison with the theory

Recall that in experiments, the nanocluster suspension flows through a closed loop circuit and passes several times through the filter. When the nanoclusters are progressively captured by the filter, their concentration ϕ decreases with time in all points of the connecting tube.

In Fig. 4a, we plot the relative concentration of nanoclusters, ϕ/ϕ_0, as function of the dimensionless time T for two values of the filtration speed u at a fixed magnetic field, H_0=16 kA/m, while Fig. 4b shows the same dependencies at a fixed filtration speed, u=0.03 m/s and for two values of the magnetic field, H_0. Qualitatively, the curves of Fig. 4 show that the filtration process accelerates as the Mason number $Ma \propto u / H_0^2$ decreases, in qualitative accordance with the theory [Eq. (8)]. As the filtration speed decreases, the nanoclusters have enough time to enter into contact with the collectors and therefore be captured. Furthermore, as the magnetic field increases, the attraction between both species is amplified. To check if all nanoclusters were removed from the circuit at the end of the filtration, the samples are

analyzed by the dynamic light scattering (DLS). All the experiments at non zero magnetic field showed transparent samples at the end of filtration, and the DLS did not detect particles in the sub-micron size range. The suspension was therefore filtrated until a concentration below the detection limit of the DLS device equal to 10^{-6}vol.% or $5{\cdot}10^{-5}$ g/l.

The capture efficiency Λ of the clean filter can be obtained by fitting the experimental curves $\phi(t)$ with the macroscopic filtration law [Eq. (5)]. Such a fit is shown by solid lines Figs. 4a and 4b. Firstly, we remark that the macroscopic filtration law agrees with the experiments.

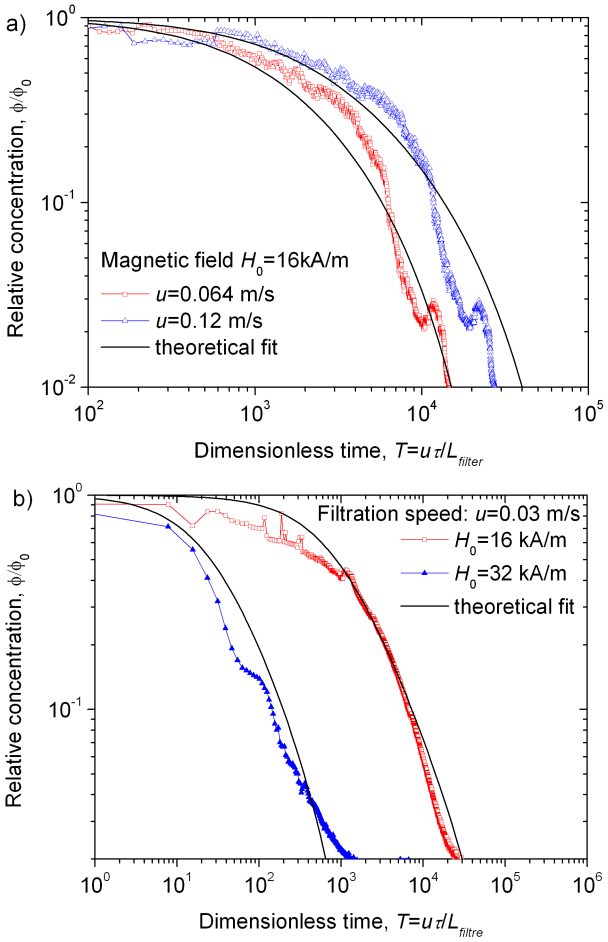

Fig. 4. (Color online) Fit of experimental time dependencies of the concentration by the macroscopic filtration law [Eq. (5)]: (a) constant field and varying speeds; (b) constant speed and varying fields. For both cases, the initial concentration of the solid phase is ϕ_0=0.0016%vol.

Fig. 5 shows the experimental dependency of the capture efficiency Λ (drawn from the fit of the experimental curves) on the Mason number. The experimental dependency is compared with the theoretical one [Eq. (8)] in the same figure. As inferred from this figure, the experimental capture efficiency undergoes a rather strong decrease at weak Mason numbers $Ma<10^4$, followed by a slower decrease at higher Mason numbers, $Ma>10^4$. The

strong decrease of the efficiency occurs in the range of the magnetic fields $16<H_0<32$ kA/m. Microscopic visualisations and analysis of the suspension phase diagram[5] show that the suspension undergoes a "gas-liquid" colloidal phase transition at the magnetic field about H_0=20kA/m and at the considered solid phase concentration ϕ_0=0.0016%. This transition is manifested by a formation of nanocluster aggregates in the suspension bulk. The aggregates have a bigger size than the isolated nanoclusters, so they are more efficiently captured by the filter collectors. The phase separation does not take place at H_0=16kA/m such that the capture efficiency is drastically decreased as compared to that at H_0=32 kA/m (compare the first labelled point with the last three points in Fig. 5). Our model does not take into account eventual aggregation of nanoclusters, so we should not compare the first experimental point with experiments, keeping in mind that the physics of capture is much more complicated than that described by the model.

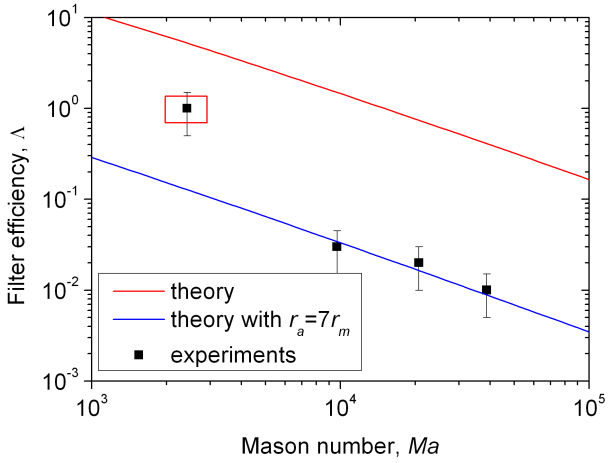

Fig. 5 (Color online). Comparison between the theoretical and experimental filter efficiency as function of Mason number. The experimental point labelled by a red rectangle stands for eventual phase separation in the suspension of nanoclusters at the applied magnetic field H_0=32 kA/m

We notice that the theory based on approximation of isolated nanoclusters (red curve) overestimates the capture efficiency by one order of magnitude for $Ma>10^4$. This discrepancy could be explained by formation of collector agglomerates inside the filter because of magnetic interactions between them. Such a reorganisation is possible in our filter of the porosity $\varepsilon\approx0.7$. This would restrict the penetration of nanoclusters inside the agglomerates. At this condition, the elementary collector is no more a microsphere of a radius r_m but an agglomerate (composed of several microspheres) of an effective size $r_a>r_m$. The formation of agglomerates would reduce the effective number of individual collectors and would decrease the filter efficiency. The simplest way to take into account this effect in our theory consists of replacing r_m by r_a in equations (6)-(8). This leads to the following expressions for the filter

efficiency: $\Lambda_a = \left(r_a / r_m\right)^{-1.83} \Lambda$ at $10^2 < Ma < 10^4$ and $\Lambda_a = \left(r_a / r_m\right)^{-2} \Lambda$ at $10^4 < Ma < 10^6$, where the capture efficiency Λ is defined by Eq. (8).

Choosing the ratio r_a/r_m~7, we manage to superimpose the corrected theoretical curve (blue curve) with the three experimental points obtained for the magnetic field H_0=16 kA/m. Thus, the corrected theory is capable to predict the behaviour of the filter efficiency as function of the Mason number at low enough magnetic fields (or dipolar coupling parameters α), for which there is no phase separation in the suspension bulk.

V. Conclusions

We have studied the magnetic nanocluster capture by a porous medium composed of a bed of magnetized spheres. In experiments with the closed loop filtration, the nanocluster concentration ϕ decreases progressively with time thanks to the capture of the nanoclusters by the microspheres. One of the mechanisms governing the nanocluster capture in the porous medium is connected to the interplay between the hydrodynamic and magnetic forces exerted to the nanoclusters. This mechanism is described by the ratio of these both forces – the Mason number Ma. An additional mechanism reinforcing the capture efficiency can be attributed to the phase separation in the suspension bulk within the known range of the parameters α and ϕ. The filtration efficiency Λ is characterized by the ratio of the nanocluster concentrations at the filter inlet and outlet and follows the power-law trend $\Lambda \propto Ma^{-0.83}$ in the range $10^2<Ma<10^4$ and $\Lambda \propto Ma^{-1}$ at $Ma>10^4$ for $\phi \leq 0.0016\%$ and $\alpha \leq 5$. Our theoretical model allows a correct prediction of the Mason number behaviour of the filter efficiency in the above range of the dimensionless parameters.

Acknowledgments

This work has been supported by the project "Factories of the Future" (grant No. 260073, DynExpert FP7) and by the project PICS 6102 CNRS/Ural Federal University.

References

[1] J. Svoboda, *Magnetic Techniques for the Treatment of Materials* (Kluwer Academic Publishers, Dordrecht, 2004).

[2] M. Zborowski and J. J. Chalmers, *Magnetic Cell Separation* (Elsevier, Amsterdam, 2008).

[3] R. D. Ambashta and M. Sillanpää, J. Hazard. Mater. **180**, 38 (2010).

[4] G. D. Moeser, K. A. Roach, W. H. Green, T. A. Hatton, and P. E. Laibinis, AIChE J. **50**, 2835 (2004).

[5] C. Magnet, P. Kuzhir, G. Bossis, A. Meunier, L. Suloeva, and A. Zubarev, Phys. Rev. E **86**, 011404 (2012).

[6] C. Magnet, P. Kuzhir, G. Bossis, A. Meunier, S. Nave, A. Zubarev, C. Lomenech and V. Bashtovoi, Phys. Rev. E **89**, 032310 (2014).

[7] R. Gerber and R. R. Birss, *High Gradient Magnetic Separation* (Research Studies Press, New York, 1983).

[8] C. Tien, and B. V. Ramarao, *Granular Filtration of Aerosols and Hydrosols* (Elsevier Science & Technology Books, New York, 2007)

[9] J.P. Herzig, D. M. Leclerc, and P. Le Goff, Ind. Eng. Chem., **62**, 8 (1970)

[10] J. Happel, AIChE J. **4**, 197 (1958).

[11] C. Moyer, M. Natenapit, and S. Arajs, J. Magn. Magn. Mater. **44**, 99 (1984)

[12] F.J. Friedlaender, R. Gerber, W. Kurz, and R.R. Birss, IEEE Trans. Magn. **17**, 2804 (1981)